Understanding nanopore window distortions in the reversible molecular valve zeolite RHO

Balestra, S.R.G.; Hamad, S.; Ruiz-Salvador, A.R.; Domínguez-García, V.; Merkling, P.J.; Dubbeldam, D.; Calero, S.

DOI
10.1021/acs.chemmater.5b02103

Publication date
2015

Document Version
Final published version

Published in
Chemistry of Materials

License
Article 25fa Dutch Copyright Act

CHEMISTRY OF MATERIALS

Article

pubs.acs.org/cm

Understanding Nanopore Window Distortions in the Reversible Molecular Valve Zeolite RHO

Salvador R. G. Balestra,[†] Said Hamad,*[,†] A. Rabdel Ruiz-Salvador,[†] Virginia Domínguez−García,[‡] Patrick J. Merkling,[†] David Dubbeldam,[¶] and Sofía Calero*[,†]

[†]Área de Química−Física, Universidad Pablo de Olavide, Ctra. Utrera km 1, 41013 Seville, Spain

[‡]Departamento de Electromagnetismo y Física de la Materia, and Instituto Carlos I de Física Teórica y Computacional, Universidad de Granada, 18071 Granada, Spain

[¶]Van't Hoff Institute for Molecular Sciences, University of Amsterdam, Science Park 904, 1098 XH Amsterdam, The Netherlands

Supporting Information

ABSTRACT: Molecular valves are becoming popular for potential biomedical applications. However, little is known concerning their performance in energy and environmental areas. Zeolite RHO shows unique pore deformations upon changes in hydration, cation siting, cation type, or temperature−pressure conditions. By varying the level of distortion of double eight-rings, it is possible to control the adsorption properties, which confer a molecular valve behavior to this material. We have employed interatomic potentials-based simulations to obtain a detailed atomistic view of the structural distortion mechanisms of zeolite RHO, in contrast with the averaged and space group restricted information provided by diffraction studies. We have modeled four aluminosilicate structures, containing Li^+, Na^+, K^+, Ca^{2+} cations. The distortions of the three different zeolite rings are coupled, and the six- and eight-membered rings are largely flexible. A large dependence on the polarizing power of the extra-framework cations and with the loading of water has been found for the minimum aperture of the eight-membered rings that control the nanovalve effect. The calculated energy barriers for moving the cations across the eight-membered rings are very high, which explains the experimentally observed slow kinetics of the phase transition as well as the appearance of metastable phases.

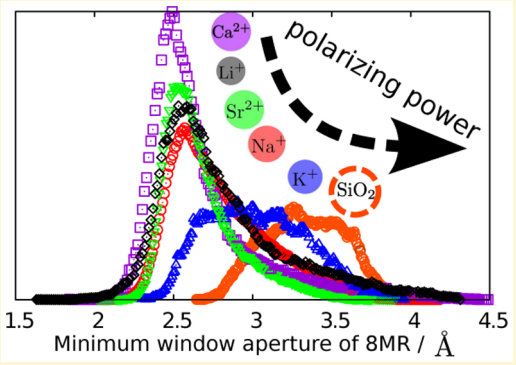

INTRODUCTION

Molecular valves are a class of molecular devices that allow molecular transport in a controlled way through gate opening or trapdoor mechanisms. Valve action is typically performed by a molecule that is attached to the material, either by covalent bonds, hydrogen bonds, or supramolecular interaction. In the presence of external stimuli, such as temperature, pressure, pH, or molecular or ion chemical potential, this molecule is able to change its configuration to allow the molecular flow. This ability has attracted huge attention during the last years due to its impact in delivering medium and large size active molecules for medical applications.[1−4] However, for small molecules, such as carbon dioxide or small hydrocarbons, operating the molecular valve through an attached molecule is less suitable, as a higher structural control is required for this kind of molecules. In this context, zeolites and metal−organic frameworks (MOFs) appear as candidate materials due to their crystalline nature and their smaller nanopore windows. Since zeolites and MOFs exhibit molecular sieving properties, the conjunction of these properties with particular structural flexibility can give rise to molecular valve behavior.

Kuznicki et al.[5] were pioneering in showing that efficient separation of small molecules can be achieved by exploiting framework flexibility. In these selected frameworks, pore window diameters can be tuned by means of temperature to separate O_2:N_2, N_2:CH_4, and CH_4:C_2H_6 mixtures. Zeolite RHO has a reversible operating mechanism, which can be controlled to smoothly switch from one stable form to another by exposure to vacuum, dehydration, and changes in temperature.[6−12] Its potential use in applications that make use of the molecular sieving of small molecules is huge, making this zeolite an excellent case for the study of thermally resistant and highly flexible materials (see Figure 1). Indeed, Lozinska et al. studied recently CO_2 adsorption and separation in several forms of univalent metal-exchanged zeolite RHO[13] and found that the Na-form is the best candidate for applications in selective kinetic gas separation of CO_2. They performed adsorption experiments, combined with crystallographic analysis, which showed that the observed molecular sieving behavior is due to a molecular valve effect associated with the extra-framework cations (EFCs) that control the molecular passage through windows between cages. This is a key aspect involved in the

Received: June 1, 2015
Revised: July 13, 2015
Published: July 14, 2015

DOI: 10.1021/acs.chemmater.5b02103
Chem. Mater. 2015, 27, 5657−5667

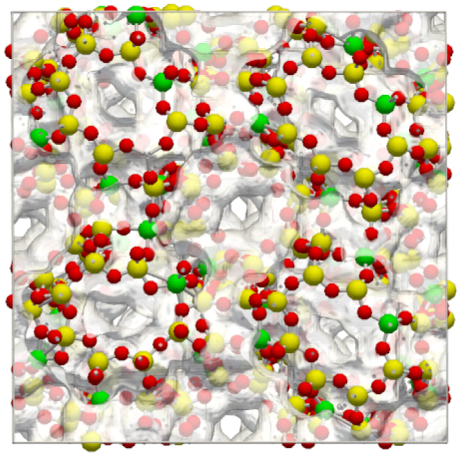

Figure 1. Snapshot of a distorted form of RHO-type zeolite obtained by molecular dynamics. An isoenergy surface is shown in translucent gray. EFCs are omitted for clarity.

high selectivity of this material for CO_2:CH_4 separation. In another recent paper, Palomino et al.[12] showed that in a mixed Na−Cs zeolite RHO, a reversible phase transition from I$\bar{4}$3m (No. 217) to Im$\bar{3}$m (No. 229), and vice versa, can be driven by the presence of adsorbed CO_2 molecules. They found that this zeolite exhibits the highest selectivity toward CO_2:CH_4 separation, which was related to the polarity of the framework (ratio Si/Al = 4.5) and the pore opening due to the phase transition triggered by CO_2 adsorption.

The aluminosilicate zeolite RHO, which adopts an Im$\bar{3}$m centric structure for temperatures above 300 K, undergoes a significant pore distortion at lower temperatures, which results in the stabilization of the I$\bar{4}$3m acentric form (Figure 2b). To

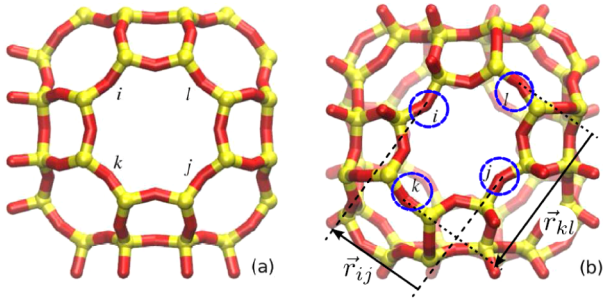

Figure 2. Zeolite RHO in the (a) Im$\bar{3}$m and (b) I$\bar{4}$3m space groups. r_{ij} and r_{kl} are used for measuring the distortion parameter Δ as defined in eq 1.

quantify the degree of distortion, Parise and Prince[14] introduced a measure that relates the average value of the degree of ellipticity of the double eight-rings (D8R), describing the pore opening windows, as shown in eq 1:

$$\Delta = \frac{1}{2}\langle |r_{ij} - r_{kl}| \rangle \quad (1)$$

where $r_{ij} = \|\vec{r}_i - \vec{r}_j\|$, and i, j, k, and l are defined in Figure 2.

It has been found that zeolite RHO, upon insertion of divalent cations, undergoes an abrupt structural change toward the acentric form,[6] with 2−6% changes in the cell parameters and Δ values of ∼2 Å in in the acentric form. This is in contrast with the smoother behavior found in the monovalent exchanged zeolite RHO, which exhibits changes in the cell parameters ∼3% lower and has lower values of the Δ parameter (ca. 1.5 Å).[11] It is worth noting that the appearance of framework distortions in deuterated zeolite RHO[9] suggests that this behavior is inherent to the framework topology. This observation is in agreement with our previous paper,[15] in which we showed, by means of interatomic potential-based energy minimizations, that pure silica zeolite RHO has two stable forms (with Δ = 0 and Δ≠ 0), and it could experience a phase transition between them (from I$\bar{4}$3m to Im$\bar{3}$m space group) at high temperatures. This result was supported by the calculations of X-ray diffraction patterns.[15] These results suggest that the EFCs might act as modulators of the framework distortions observed in zeolite RHO containing EFCs.

The structural picture discussed earlier, which is also used to explain the molecular sieving properties of the mentioned works, rests on the averaged and space-group restricted information retrieved by diffraction techniques. Computer modeling offers the opportunity to overcome these limitations and hence to provide a deeper insight into the distortion mechanisms. In the present context, this is of particular relevance since the mechanism involved in the molecular valve behavior in zeolites and related materials is still poorly understood. We must note that zeolite RHO has been investigated in the past by molecular simulation techniques. Using the standard distance least-squares procedures, Baur et al.[16] showed that the degree of ellipticity of 8MRs is strictly a function of the cell parameters. In other simulation study, Bieniok et al.[17,18] analyzed the phase transition of a set of RHO-forms using an approximation (rigid unit modes, RUM) and found some possible additional low-energy framework transformations. These three studies have some limitations in terms of the validity of their predictive capability since they are not able to consider atomistically the EFCs.

In this work, we carry out a detailed atomistic simulation study to gain a better understanding of the relationship between the nature of the EFCs and the flexibility of the material, taking into account the concomitant impact on molecular sieving properties. Existing approaches for accurately modeling cation location or large variations of cell volumes in zeolites consider either poorly deformable frameworks[19−22] or those having low ratios between the cation number and their potentially accessible sites.[23−25] For all these reasons, in the early stage of this work, we were unsuccessful in reproducing the crystal structure of several cation-forms of zeolite RHO by applying these methods. For the present study, we have then developed a methodology for accurately modeling the structural behavior of crystalline nanoporous solids undergoing large structural variations, which combines cycles of Monte Carlo (MC) calculations, energy minimization (EM), and molecular dynamics (MD) simulations. To study the effect of the ionic polarizing power, that is, the ionic charge/size ratio, five metal-forms (Na^+, Li^+, K^+, Ca^{2+}, and Sr^{2+}) of zeolite RHO were considered. The behavior of the pore windows deserves particular attention, as it is expected to be strongly associated with the nanovalve behavior linked to three main phenomena, namely adsorption, separation, and transport properties.

COMPUTATIONAL SECTION

The methodology used here for the realistic structural modeling of zeolite RHO is inspired by the experience in modeling massively defective ionic solids,[26,27] in which large structural deformations occur. Since one of the results of this research has been the development of

DOI: 10.1021/acs.chemmater.5b02103
Chem. Mater. 2015, 27, 5657−5667

the new methodology, it is presented in the next section, along with the rest of the results. As anticipated earlier, several modeling cycles will be carried out, and therefore the use of first-principles calculations is hindered by its CPU cost. Thus, interatomic potentials-based simulations are the method of choice. For the case of zeolite RHO, in particular to model the acentric phase, we noted that the shell model is required to take into account the polarizability of the framework oxygen atoms. To check the importance of polarizability on the structure, several trial configurations of metal-forms of zeolite RHO having acentric $I\bar{4}3m$ structures were modeled. While the acentric structure was kept during energy minimization, it changed to centric $Im\bar{3}m$ when the shell constant was gradually increased to reach very high values. These high values of the shell constant would make the atoms behave as nonpolarizable atoms. In addition, we used the rigid-ion models of Van Beest et al.[28,29] and Ramsahye and Bell,[30] for which the acentric structure is not stable either. Then, the well-known shell-model potentials of Sanders et al.[31] were used, as they provide accurate structures of complex zeolites. In connection with it, Li^+, Na^+, K^+, Ca^{2+}, and Sr^{2+} cations were selected considering the existence of good quality interatomic potentials[32−34] that are compatible with the Sanders et al. potentials.

At the experimental synthesis temperature, RHO zeolites adopt the centric cubic $Im\bar{3}m$ structure, with only one distinct tetrahedral site in the asymmetric unit cell,[35,36] which strongly suggests that a particular ordering of the Al atoms is not likely to occur. In addition, RHO zeolites are synthesized with monovalent cations, usually mixtures of Na^+ and Cs^+. There is no need to introduce the close pairs Al−Al that would be required if divalent cations were used.[37] Therefore, like in the case of FAU zeolites,[38] Al atoms in RHO zeolites are expected to stay as far as possible from each other, following Dempsey's rule,[38] as was recently shown to be expected to hold in zeolites unless framework anisotropy perturbs this behavior.[39] To analyze the influence of Al location in the unit cell, we constructed two different configurations distributing the Al atoms as follows: (a) as far as possible in a 2 × 2 × 2 supercell, and (b) as far as possible in a single unit cell, which was subsequently expanded to a 2 × 2 × 2 supercell.

Zeolites are known to contract upon dehydration, which in part is due to the loss of space filling molecules but more importantly to the increased electrostatic attraction of the EFCs.[40] Zeolite RHO experimental results have shown that the cell contraction caused by dehydration is accompanied by a phase transition from centric to acentric form.[8,14,41] Then, with the aim of determining whether the cell contraction per se causes the phase transition of the RHO zeolite framework, we modeled the effect of the externally applied pressure on the pure silica structure. Previous work has shown that the chosen potentials perform very well on aluminosilicate zeolites subject to high pressures.[42] This is also a test for the applicability of the potentials to model the lower acentric symmetry of zeolite RHO.

Lozinska et al.[41] have found that, once dehydrated, the monovalent forms of zeolite RHO do not change from the acentric to the centric space group when the temperature increases. To get better atomistic insight into this interesting result, we have conducted three computational experiments. The first two concern the study of the influence of water and EFCs in the structural features of zeolites.[40,43] In the first study, water was initially considered as a continuum dielectric medium that screens cation−zeolite Coulombic interactions with the aim of understanding the structural features of complex zeolites upon progressive dehydration. In the second study, water molecules were treated explicitly. Moreover, we calculated the energy barriers that the cations should surpass when traveling across the zeolite windows to go from one cationic site to another.

To quantify the degree of distortions, we used the following parameters:

$$\delta_4^t = \frac{1}{2}\left|r_{ik}^t - r_{jl}^t\right| \tag{2}$$

$$\delta_6^t = \frac{1}{2}\left|\max(r_{il}^t, r_{jm}^t, r_{kn}^t) - \min(r_{il}^t, r_{jm}^t, r_{kn}^t)\right| \tag{3}$$

$$\delta_8^t = \frac{1}{2}\max\left(\left|r_{im}^t - r_{ko}^t\right|, \left|r_{jn}^t - r_{pl}^t\right|\right) \tag{4}$$

where $r_{ij}^t = \|\vec{r}_i(t) - \vec{r}_j(t)\|$, and i, j, k, ... o, p are oxygen atoms labeled clockwise. These parameters are defined for each window (4, 6, and 8-rings) and time t (e.g., for 8-ring see Figure 2). Thus, we calculate average values for all windows and time:

$$\Gamma \equiv \langle\delta_4\rangle, \quad \Lambda \equiv \langle\delta_6\rangle, \quad \Delta \equiv \langle\delta_8\rangle \tag{5}$$

Eq 4 is a generalization of the degree of ellipticity of D8R, originally described as in eq 1. This is motivated by a previous experimental work on zeolite LTA,[44] where a complex behavior for the window distortion was observed. Eq 4 was defined in a previous work;[14] however, eqs 2 and 3 are first introduced in the present work. A state-of-the-art algorithm was used for the automatic nontrivial identification of all window-types,[45] which is based on loops searching in empirical networks treating each zeolite window as a loop in a dynamic graph. In addition to the three distortion parameters (Γ, Λ, and Δ), the average cell parameter allows us to monitor the geometry of the unit cell during the simulations. For computing the average values extracted from the simulations and reported in the following, ergodicity has been assumed, and therefore the average values are calculated as the corresponding ensemble average.[46,47] In this way, the more stable configurations have a larger stability and contribute more to the computed observables.

The MC simulations have been carried out using the code RASPA,[48] while the EM and MD ones have been carried out using the GULP code.[49] Constant pressure MD simulations with isotropic volume fluctuations and fully flexible unit cells have been used to study the evolution of the system and to produce the correct statistical ensemble (Nosé−Hoover thermostat with Rahman−Parrinello barostat[50]) since it allows for phase changes in the simulation. In the MD simulations, the pressure has been set to zero. The integration time step is 0.1 fs. Each MD step consisted on a 2.5 ps equilibration simulation, followed by a 2.5 ps production run. Electrostatic interactions are calculated using the Ewald summation.[51,52] A cutoff radius of 12 Å is used for short-range interactions.

RESULTS

To model a system that is comparable to those studied experimentally, we considered the inclusion of Al atoms. To do that, two crystalline configurations are set up, replacing 80 Si atoms by 80 Al atoms (per computational box, consisting of a 2 × 2 × 2 supercell). The Al atoms are placed in such a way that first, they obey Löwenstein's rule,[53] and second, the Coulombic repulsions between Al-centered tetrahedron are minimized. The first configuration is labeled as C1 and has the Al atoms placed as far as possible in a 2 × 2 × 2 supercell. The average distance between Al atoms is $\langle \mathrm{Al}_i\ \mathrm{Al}_j\rangle_{C1}$ = 14.49 Å, and the average distance between the closest pairs of Al atoms is $\langle C(\mathrm{Al}_i\mathrm{Al}_j)\rangle_{C1}$ = 5.73 Å. The second configuration (C2) is constructed by placing the Al atoms as far as possible in a single unit cell, which is subsequently expanded to build a 2 × 2 × 2 supercell. The average distances between Al atoms and between closest Al pairs are $\langle \mathrm{Al}_i\ \mathrm{Al}_j\rangle_{C2}$ = 14.50 Å and $\langle C(\mathrm{Al}_i\mathrm{Al}_j)\rangle_{C2}$ = 5.64 Å, respectively. C2 has a higher symmetry than C1, so the average distance between closest pairs of Al atoms is about 0.1 Å higher. This is just a small increase, which suggests that it is not necessary to employ the larger unit cell to model the system correctly since the small improvements that would be achieved by increasing Al−Al repulsions would be insufficient to compensate for the increase in simulation time. We will therefore use the configuration C1 for the rest of this work. The atomic coordinates of the framework atoms (Si, Al, and O atoms) of both structures are provided in the Supporting Information.

DOI: 10.1021/acs.chemmater.5b02103
Chem. Mater. 2015, 27, 5657−5667

The strong attractive interaction between the EFCs and the oxygen atoms of the zeolite exerts a large force on the framework that is likely to be the cause of the phase transition from the centric $Im\bar{3}m$ to the acentric $I4\bar{3}m$ structure with the concomitant reduction of the cell volume and the increase of the pore window acentricity (Δ parameter). To shed more light on this feature, we analyzed the behavior of the pure silica zeolite RHO in the presence of an externally applied pressure. Figure 3, left panel shows that, indeed, framework volume

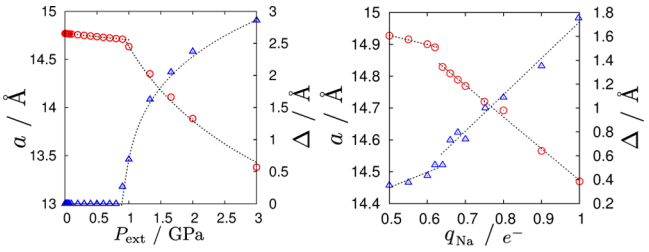

Figure 3. Left: cell parameter, a (°), and 8MR window distortion, Δ (△) versus applied external pressure, for pure silica zeolite RHO. Right: cell parameter and 8MR window distortion, for Na-RHO, versus partial charge for sodium cations, q_{Na}. We observe a structural phase transition at 1 GPa and q_{Na} = 0.62 e^-, respectively. The errors are smaller than the size of the points. All regressions have $r^2 > 0.99$.

decreases gradually until a step is found at 1 GPa. At this point, the acentricity parameter is 0.25 Å, and the crystal structure adopts the acentric form. This explains the origin of the phase transition of zeolite RHO. In the remaining of the paper, we will explore it to greater depths as well as the structural features related to the cell deformation and their impact on the molecular nanovalve effects.

In a previous work, it was shown that a qualitative picture of the role of the EFCs in the zeolite structural deformation can be obtained by mimicking the screening effect of water by decreasing the charge of the EFCs.[40] The curve displaying the variations of the cell parameter as a function of the charge of the cation is shown in Figure 3, right panel for Na-RHO. We observe again a gradual variation, followed by a step where the acentricity parameter undergoes a large change. The symmetry also changes from the centric to the acentric space group. The decrease of the charge of the cations could be regarded as an increase in water content and is accompanied by a reduction of cation−oxygen interactions and consequently by larger interatomic distances. [40] This can cause the migration of cations, which indeed moved from Site I to Site II.

For a realistic modeling of highly flexible porous nanoporous solids, we have used a methodology with which to achieve a step by step approach toward the most likely structure of these complex materials. Zeolite RHO, according to experimental evidence, is among those nanoporous materials where there are many available sites for cation siting, and a close coupling exists between cation siting, cell parameters, and crystal symmetry. In this case, it is not possible to find an initial structural model that leads to a realistic description of the zeolite through a single-step molecular simulation method (EM, MC, or MD). This is a consequence of the very complex surface energy, and thus any random trial is likely to change the structure around the closest local minimum. To surmount this, we aimed to design a method that would be able to approach the structure in an adaptive way. This methodology combines MC, EM, and MD in iterative cycles. A schematic view of the method is shown in Figure 4. This scheme shows the main feature of the method, which is the cyclic nature of the MC/EM/MD steps. The

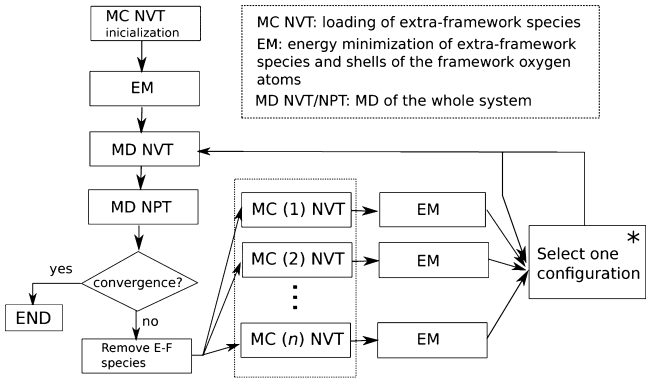

Figure 4. EM/MC/MD simulation scheme used in this work. (∗) We select the most stable configuration, according to their Boltzmann weights, among the previously accepted configuration and a new set of ten trial calculated systems.

starting point is a stable framework structure, for instance the experimental structure (either solvated or desolvated), or a hypothetical structure. Ten trial MC runs are then performed to locate the extra-framework species. In the present case, these extra-framework species are EFCs or water molecules. This is followed by a lattice EM for each MC configuration, keeping the cell parameters fixed as well as the coordinates of the framework atoms. If the EM were performed allowing the cell parameters to vary, at constant pressure, the framework structure would change abruptly, and it would be trapped in a local minimum with a large distortion, from which it would be very difficult to escape. At this stage the most important issue is to achieve the relaxation of the extra-framework species, to prevent unrealistic high forces at the beginning of the MD run, which would cause the collapse of the simulation. The energies of these ten configurations along with that accepted in the previous cycle are used to select one according to Boltzmann weight as compared with a random probability. In this way, detailed balance is fulfilled.[47,54,55]

Our aim is to provide a realistic description of the material, for which thermal and entropic contributions are relevant. Since in EM calculations, these are lacking, we decided to model the overall structural changes of the solid by means of MD simulations. Then, after performing the EMs, to further ensure that the MD can be performed in a reasonable way, a short run is first accomplished at fixed cell parameters, in the NVT ensemble, followed by a long run in the NPT ensemble, with a fully flexible cell. In the later run, the cell parameters vary according to the effect of the extra-framework species and external conditions like temperature and hydrostatic external pressure. Since the coupling between the framework structure and the extra-framework species is quite strong, the MD simulation relaxes the structure primarily in accordance to the location of the extra-framework species. Moreover, in this MD stage, some extra-framework species can surpass the local energy barriers and move to adjacent stable cation/adsorbate sites. This movement to other cation/adsorbate sites causes in turn changes in the framework and the overall structure of the material. After each MD run, the obtained framework structure is taken for the new cycle, while the extra-framework atoms are removed and inserted back with the MC scheme step. This

DOI: 10.1021/acs.chemmater.5b02103
Chem. Mater. 2015, 27, 5657−5667

cyclic process is repeated iteratively until the potential energy of the system is equilibrated.

Figure 5 shows the evolution of potential energy and cell size, as when the described method is employed to model zeolite

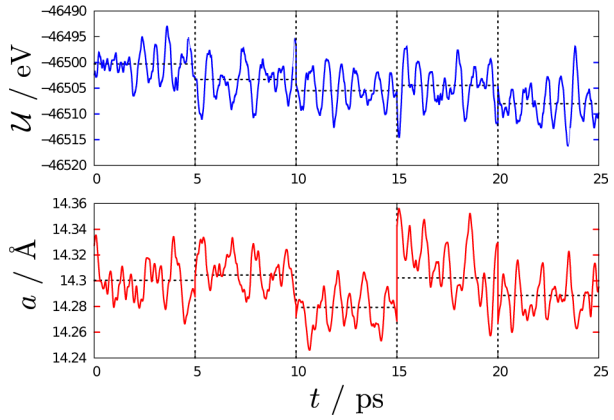

Figure 5. Variation of the potential energy (top) and cell size (bottom) with the number of MD simulation steps, for the first five MC/EM/MD cycles, for Sr-RHO. Horizontal dashed lines represent the average potential energy and cell size, respectively. Vertical dashed lines represent boundaries between cycles. The temperature is 300 K.

RHO with Sr^{2+} cations. For clarity reasons, only the first five MD/EM/MC cycles are shown (for the complete curve, see Figure S4, Supporting Information). At the beginning of each MC/EM/MD-cycle, there is a sudden increase in the cell parameters resulting from the repulsion induced by the EFCs located in new sites with respect to their previous positions. The response of the whole system is to slightly increase cation−zeolite distances, while at the same time the structure is relaxed. During the transit along the MC/EM/MD cycles, the internal energy, that is, the average of total potential energy, decreases and converges. We observe that the potential energy tends to decrease as the methodology proceeds. However, the behavior of the cell size is complex, which is a consequence of the structural variation of the system trying to gain stability upon relocation of the EFCs in each MC step. In fact, this is the core point of our methodology.

We have employed the MC/EM/MD algorithm to study the dependence with temperature of the cell size for all cations. The results obtained in our simulations, as well as the available experimental data, are reported in Table 1. We have simulated zeolites containing 80 and 92 aluminum atoms per simulation cell, with Si/Al ratios of 3.8 and 3.17, respectively, to compare with experiments. We observe negative thermal expansion (NTE) in all cases, but unlike what Reisner et al.[8] reported, our results suggest that the negative thermal expansion is not associated with a gradual dehydration but the intrinsic response of the dehydrated aluminosilicate to an increase of temperature. It is worth noting also that the pure silica hypothetical zeolite RHO shows NTE. In relation to this point, the collapse of the structures with high polarizing powers occurs due to the limitation of the potentials, but the main picture is well described, as the same behavior is observed experimentally but at higher temperatures. Finally, it is worth noting that the difference of the computed cell parameters with experiments is below 0.2%. This is the first theoretical work that achieves such a close agreement with experimental data in a highly flexible zeolite containing Al atoms and EFCs.

In connection with the earlier results, here we address the EFCs location and the population of the different cationic sites, as obtained from our simulations. Experimentally, three crystallographic sites are known for EFCs in zeolite RHO:

Table 1. Dependence on Temperature of the Average Cell Parameter, *a*, for Silica and Aluminosilicate Forms of RHO-type Zeolites

T_{ext} (K)	⟨*a*⟩ (Å ± 0.001 Å)	Exp. [ref]	⟨*a*⟩ (Å ± 0.001 Å)	Exp. [ref]	⟨*a*⟩ (Å ± 0.001 Å)	Exp. [ref]	⟨*a*⟩ (Å)
Me−RHO$_{n_{Al}}$	Na_{80}		K_{80}		Ca_{80}		SiO_2
100	14.619		14.964		14.379		14.757
200	14.554		14.722		14.195		14.635
300	14.431	14.4139[13]	14.602	14.5951[13]	14.141		14.487
		14.3771[41]		14.5959[41]			
350	14.475		14.650		14.004		14.395
500	14.467		14.613		collapsed		14.438
600	14.423		14.805		collapsed		
	Li_{80}		Sr_{80}		Na_{92}		
100	14.491		14.429		14.340		
200	14.330		14.388		14.103		
300	14.208	14.2448[13]	14.402		14.141		
350	14.102		14.352		14.004		
500	collapsed		14.173		collapsed		
600	collapsed		14.187		collapsed		
	K_{92}		Ca_{92}		Sr_{92}		
100	14.747		14.340		14.382		
200	14.669		14.203	14.489	14.412		
300	14.607		14.058	14.45[6]	14.327	14.45[6]	
500	14.498		collapsed	14.01[6]	14.259	14.56[6]	
						14.05[6]	
600	14.498		collapsed	14.07[6]	14.211	13.98[6]	

DOI: 10.1021/acs.chemmater.5b02103
Chem. Mater. 2015, 27, 5657−5667

(site I) inside a double 8-ring, (site II) at the center of a single 8-ring, and (site III) in front of the 6-ring (see Figure 6). In

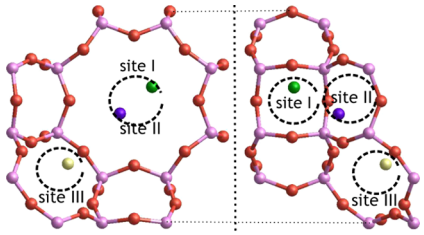

Figure 6. Atomistic view of the cationic sites in zeolite RHO. Sites I–III depicted as dashed spheres, and their coordinates are reported below. The colored spheres represent cations in cationic sites.

agreement with the experimental data,[6,7,12,13,41] our MC/EM/MD methodology shows that most cations are distributed among the known cationic sites, while a small fraction was assigned elsewhere. This means that the latter were located outside of a 2 Å radius sphere from the reference sites, which is mainly because EFCs are found moving from one stable site to another. The population of the sites is in good agreement with experimental results, when available, considering the uncertainties associated with the experimental data that can be extracted from diffraction (see Table 2). Note, for example, that the

Table 2. Cation Site Populations in Atoms/Unit Cell within a 2 Å Radius from the Cation Sites at Temperature 300 K[a]

cation	site I	site II	site III	elsewhere
Na_{80}	1.64	6.55	1.61	0.08
Exp. 41		6.48	3.00	
Na_{92}	1.36	7.09	2.94	0.07
K_{80}	2.06	5.54	2.36	0.09
Exp. 41	2.06	6.85		
K_{92}	2.08	5.91	3.39	0.10
Li_{80}	1.04	2.68	5.28	1.03
Exp. 41			8.00	
Li_{92}	1.30	3.49	5.38	1.37
Ca_{80}	2.00	1.99	0.75	0.26
Ca_{92}	3.36	2.06	0.21	0.13
Sr_{80}	1.91	2.24	0.74	0.11
Sr_{92}	3.01	2.45	0.27	0.02

[a]The experimental data about cation sites is taken from refs 7, 9, and 12, besides those taken from ref 41.

overall cation content determined in experiments varies from 80–95% of the nominal EFCs content. The largest difference was found for Li^+ with 10 cations per unit cell (80 cations per simulation cell), where experiments allocated eight of these atoms to site III, whereas we found 5.3 atoms at this site, 2.7 at site II, 1.0 at site I, and 1.0 elsewhere. The sum of the populations of sites II and III matches very well the experimental value obtained for the latter site. This is located near site II, and considering the large uncertainty that can be associated with the location of Li^+ cations by X-ray diffraction, we can conclude that the simulations provide a reasonable agreement with experiments. When the number of cations increases, concomitant with the increase of Al-atoms per unit cell from 10 to 11.5, we obtain that the occupation of site III increases for Na^+ and K^+, while for the case of Ca^{2+} and Sr^{2+}, this site depopulates in favor of site I. The success in reproducing both the cell parameter behavior and the EFCs location provides confidence in the ability of our calculations to correctly describe the complex behavior of zeolite RHO and analyze in detail the dynamical features of the pore window and its connection to nanovalve effects.

Since the methodology does not impose any symmetry constraints other than the supercell, it is able to provide structural and dynamical data that are close to the behavior of the materials. This can be exploited for increasing our understanding of this complex behavior, in particular in materials with a large degree of flexibility such as zeolite RHO. Previous simulation work[56−58] has shown that, even for rather rigid zeolites, the size of the windows that delimit the pore opening has large deviations (ca. 0.4 Å) due to the thermal motion. Diffraction studies cannot capture this feature accurately due to the symmetry-averaged picture it provides, even by analyzing the information extracted from the Debye−Waller factors. In the present context, it is useful to note that despite the role that the flexibility of the windows plays in the transport properties of zeolites without EFCs,[56−58] how the windows flexibility is modified in the presence of EFCs remains unexplored. As we have shown above, we have confidence in the accuracy of the developed computational scheme to provide accurate structural data, and therefore we can enter into the detailed analysis of the window deformations for the different metal-forms of zeolite RHO.

As reported by Deem et al.,[59] MD simulations serve as a useful tool for studying the distortion of the windows. Figure 7 shows the window distortion profiles for pure silica and aluminosilicate forms (Li^+, Na^+, K^+, Ca^{2+}, and Sr^{2+}) by displaying the deformation parameters defined for the 4,6,8-rings (Γ, Λ, and Δ). It is worth noting that the pure silica structure shows nonzero window distortion, which is due to the thermal motion and is a fact that cannot be directly inferred by diffraction methods. We have performed ab initio MD simulations that support these findings, details of which are provided in the Supporting Information. The distortions observed for this case can be regarded as those intrinsic to the topology, and thus the deviations from them observed for the metal forms can be interpreted as being induced by the cations. Four-membered rings (4MRs) are kept mainly undistorted (Γ maximum population corresponds to Γ = 0 Å, except for pure silica structures) due to their small size, although they exhibit relatively long tails, particularly Li^+ and Ca^{2+}. Obviously, 4MRs do not directly contribute to molecular transport, but their deformation can couple to the deformation of larger windows and could enhance the pore opening of these ones. The distortions of the 6MRs are not centered at zero but at circa 0.5 Å for all forms, and they show a small dependence on the nature of the cations. This is also due to the small size of this type of window, although they have noticeably larger tails as well as a shoulder at around 1 Å for Li^+ and Ca^{2+}. In the case of 8MRs, a clear dependence of the Δ parameter with the metal polarizing power is observed. Note that for this distortion, there is a much larger departure from the behavior of the pure silica zeolite. Going back to the smaller rings, that is, 4 and 6MRs, it can be observed the effect of the polarizing power in these cases. These findings are consistent with the idea that distortions are coupled, and cations produce distortions in all rings. On this basis, it is possible to understand one interesting result of Lozinska et al.[13] who found, in their study of

DOI: 10.1021/acs.chemmater.5b02103
Chem. Mater. 2015, 27, 5657−5667

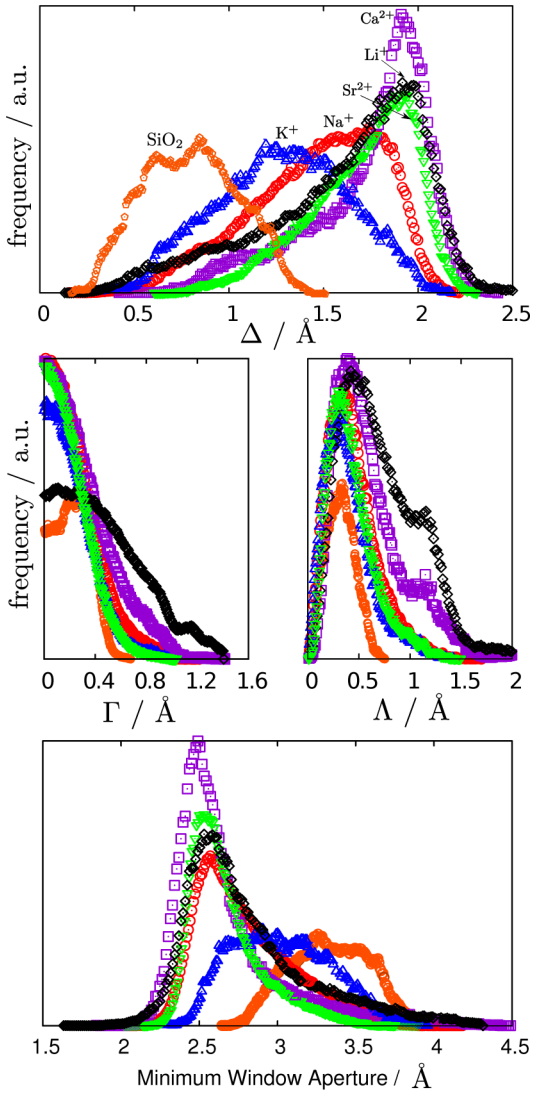

Figure 7. (Top and middle) Probability density of degree of distortion of the 4,6,8-rings (Γ, Λ, and Δ) for pure silica and aluminosilicate forms (Li^+, Na^+, K^+, Ca^{2+}, and Sr^{2+}). (Bottom) Probability density of minimum window aperture of the 8-rings for aluminosilicate forms (Li^+, Na^+, K^+, Ca^{2+}, and Sr^{2+}). The temperature is 300 K.

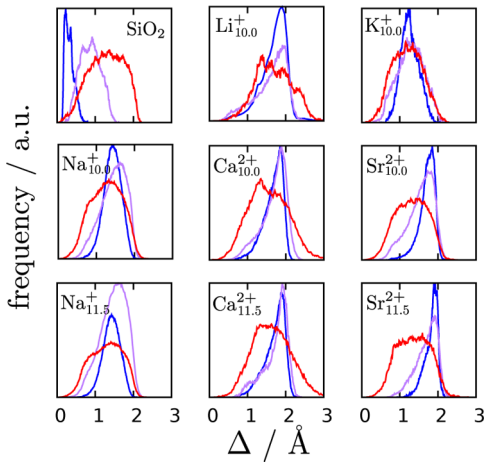

Figure 8. Probability density of degree of distortion of 8-rings for pure silica and aluminosilicate forms (Li^+, Na^+, K^+, Ca^{2+}, and Sr^{2+}) at different temperatures 100, 300, and 500 K (blue, purple, and red, respectively) and Si/Al ratios (3.8 and 3.17).

monovalent cation exchanged zeolite RHO, that despite not being located next to 8MR, the Li^+ cation is the one that induces the largest values of the mean Δ parameter. On the other hand, a direct relation between cation site occupancy and framework distortion has been found in divalent cation-exchanged zeolite RHO by Corbin et al.[6]

The behavior of the distortions in 8MRs with temperature is dependent on the nature of the metal cation present in the zeolite in a very distinct manner. For each structure with divalent cations, the distortions are about the same at 100 and 300 K, while at 500 K, the position of the maximum of the curves is reduced by about 0.5 Å, and the peak widths are doubled (Figure 8). The increase of the number of cations for these two metals has almost a negligible effect on the observed behavior, which suggests that even at the lower number of cations, their interactions with the zeolite oxygen atoms are very strong. For the monovalent cations, the influence of both the polarizing power and the number of cations is clear. Li^+ has the smallest cationic radius and thus the largest polarizing power and shows only a minor shift of the position of the maximum of the degree of distortion. The behavior of the Na^+ form shows variations with the number of cations and also with temperature. From 100 to 300 K, the distortions are larger, while they decrease at 500 K. In the case of K^+, which has the largest radius and lowest polarizing power, very little variation of the maximum of the degree of distortion is observed, even at 500 K. As was more clearly shown in Figure 7, top panel, the positions of the peaks of the distortion distributions of the three metals with largest polarizing power (Ca^{2+}, Li^+, and Sr^{2+}) do not differ in a noticeable fashion, which together with the information gained from the analysis of the temperature dependence suggests that the largest window distortion that can occur in zeolite RHO under experimental conditions is about 2 Å. The windows of pure silica zeolites exhibit increasing distortions with an increase in temperature. The overall analysis of Figure 8 reveals that at 500 K, the thermal effect makes the behavior of the window distortion independent of the nature of the cation and more dictated by the framework itself.

In agreement with Lozinska et al.,[13] for the dehydrated metal containing zeolites, we do not find a phase transition from the acentric $I\bar{4}3m$ to the centric $Im\bar{3}m$ form when the temperature increases. However, one would expect that such a phase transition might occur. To shed more light on the role of EFCs affecting the structural behavior of RHO zeolites, we analyzed the energy barrier for crossing an 8MR by mapping the energy profile of the cations moving along a path traversing the zeolite following a line that crosses the 8MR (see Figure 9) and allowing the structure to relax via EM. The data in the middle of the zeolite have no physical meaning, as cations will not get into these sites in absence of adsorbed molecules; they will rather move along the pore surface. The attention should be focused on the regions close to the zeolite windows, identified in the figure by vertical continuous lines. The centers of the D8R are represented by vertical dashed lines. We observe that the energy barriers are asymmetric, that is, they are different for forward jumps and backward jumps, except for D8R. Moreover, the relative well depth depends on the location of the Al atom in each case. The position of the first cation, for monovalent forms, is $q = 0.37$. For divalent forms, a second cation is added at $q = 0.17$.

DOI: 10.1021/acs.chemmater.5b02103
Chem. Mater. 2015, 27, 5657−5667

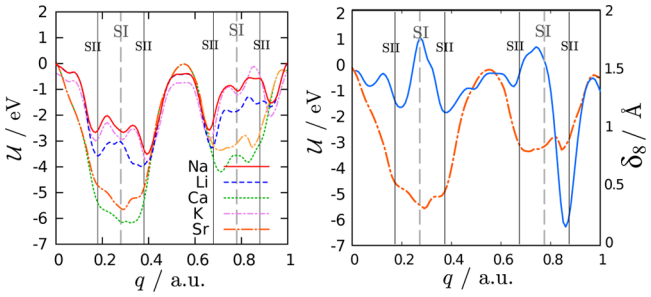

Figure 9. (Left) Potential energy landscape $\mathcal{U}$ versus reaction coordinate (in the *a*-direction through the double 8-rings), *q*, for one or two aluminum atoms per unit cell. The position of the first aluminum atom is $q = 0.37$, and the second (for the divalent cases) is $q = 0.17$, for Sr-RHO. (Right) Potential energy landscape $\mathcal{U}$ and distortion parameter δg versus reaction coordinate, *q*, for Sr-RHO form.

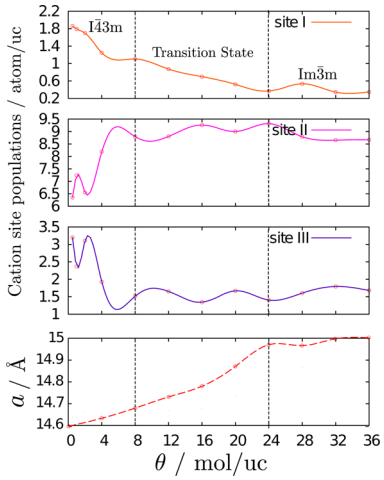

Figure 10. Top three panels: sodium site populations (at 300 K) versus loading of water, θ, for Na-RHO with 92 Na cations. Sodium site populations are measured in atoms per unit cell, within a 2 Å radius from the cation sites. Bottom panel: cell size versus water loading of Na-RHO with 92 Na cations, at 300 K.

An important conclusion we can draw from the analysis of the values of the energy barriers is that, in the dehydrated state, the cations need to overcome very high energy barriers to jump from one site to another, suggesting that phase transitions induced by cation jumps will take a very long time. This is a plausible explanation of the experimental observations of Bieniok and Baur,[18] who observed that the high temperature structure Sr-RHO quenched to 90 K and left in vacuum at room temperature, takes a week to recover the usual room temperature structure. It is interesting to note that the overall structure responds to the cation reaction coordinate, that is, when the cation is in site I of the 8-ring closest to the cation ($q = 0.27$), the degree of distortion is $\delta_8 = 1.75$. However, when the cation is in site II, $\delta_8 = 1.3$. We have not measured the degree of ellipticity induced by cations in site III. For the second D8R, δ_8 is noticeably low, at less than 0.5 for a reaction coordinate of $q = 0.85$. This indicates that the local geometry is not so much affected by the presence of the cation as it is by the simultaneous presence of the EFC and the aluminum atom of the framework. Our result could also provide a rationalization for the experimental finding that upon CO_2 adsorption in Cs-RHO, NaCs-RHO, and K-RHO, two crystal phases appear over a considerable range of gas pressures, which is likely to be a consequence of the trapping of cations in long-lived sites.[41]

In the presence of molecules that have electrostatic interactions with the zeolite, like H_2O and CO_2, it has been experimentally found that zeolite RHO can undergo reversible phase transitions.[9,12] To analyze how this process occurs, we have studied the behavior of Na-RHO for eight different water contents, from fully hydrated (36 molecules per unit cell) to completely dehydrated. We started from the fully hydrated structure, and the appropriate number of water molecules was eliminated for each case. Then, the systems were equilibrated by MD simulations. The lattice parameter of the initially completely hydrated material remains almost unchanged by removing up to one-quarter of the water molecules, reaching 24 molecules per unit cell (Figure 10, bottom). Further gradual dehydration is accompanied by a concomitant decrease of the cell parameter until all water molecules are removed. Our simulations show that the variations of the cell parameters are related to variations of the population of the cationic sites (Figure 10). A remarkable result is that at any water loading, the larger amount of cations is found in site II, whose occupation is at least two times larger than those of the other two sites. Three regions are clearly identified according to the behavior of cation site population. One corresponds to high water loading, above 24 molecules per unit cell. Another region appears at low water loadings, between zero and eight molecules per unit cell. Finally, an intermediate region is identified in between the other two. Sites I and III reach minimum occupations in the high water content region. In this case, site II is largely populated. In the intermediate region, sites II and III largely maintain their occupancies, which are similar to those in the high water content region. In contrast, site I shows a gradual decrease in the intermediate region. In the absence of water, sites I and III have the largest occupation of Na cations, while the lowest occupation is observed for site II. Upon water adsorption, after the incorporation of four molecules per unit cell, the cationic site occupancies change rapidly, and at eight molecules, sites II and III already reach the levels that are kept about constant up to the full water loading. The observed changes of cell parameters and cationic site populations modify the symmetry of the zeolite, which has the centric Im$\bar{3}$m space group for 24 water molecules per cell up to full hydration, while adopting the acentric I$\bar{4}$3m space group for eight water molecules and below.

The analysis of Figures 10 and 11 provides a more accurate view of the connection between changes in cell parameters and window distortions than that obtained earlier in this work in which water was modeled as a continuous dielectric (Figure 3, right). Figure 11 shows that the distortions of the smaller 4 and 6MRs are almost insensitive to the amount of water present and are slightly lower than those of the fully dehydrated structure. In contrast, a very large dependence of the 8MR distortion parameter, Δ, with the amount of water is observed for the interval delimited by four and 48 water molecules per unit cell (Figure 11, top). From 24 water molecules per unit cell to full hydration (36 water molecules), the distortion of 8MR does not show significant variations. This is in line with the behavior of the cell parameter and the population of the cationic sites (Figure 10). Between four and 16 water molecules per unit cell, the distribution of the Δ distortion parameter is bimodal, suggesting that some pores are closed, whereas others are open. The appearance of the double peak is due to the nucleation of water in specific sites, which is motivated by

DOI: 10.1021/acs.chemmater.5b02103
Chem. Mater. 2015, 27, 5657−5667

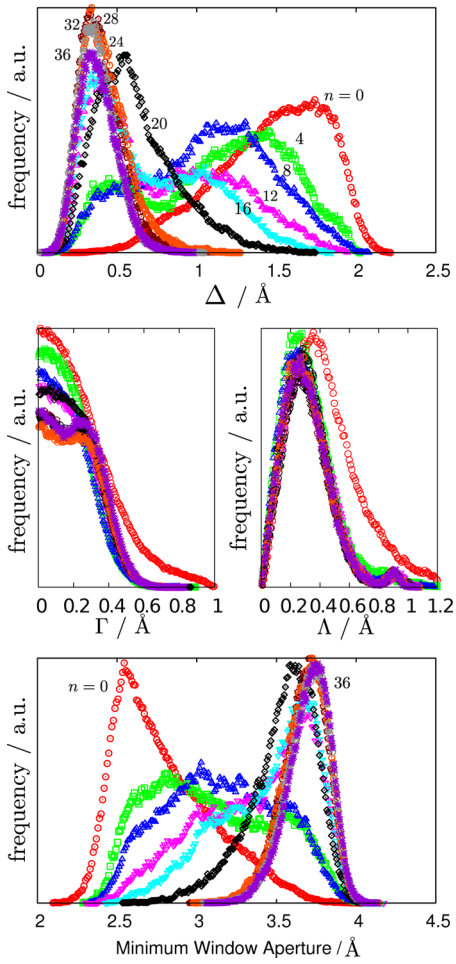

Figure 11. (Top and central) Probability density of the degree of distortion of the 4,6,8-rings (Γ, Λ, and Δ) in the presence of various amounts of water molecules and 92 Na cations, at 300 K. (Bottom) Probability density of minimum aperture of the 8-rings in the Na-RHO form in the same conditions.

strong water−water interactions. This behavior could not be predicted by the dielectric continuum model of water in Figure 3, right panel .

The structural changes occurring in an 8MR when a Na^+ cation and varying amounts of water are presented in Figure 12. We observe the large distortion of the 8MR when just one cation is present, which favors the stability of the acentric structure. The addition of water molecules induces a gradual opening of the window, leading eventually to the experimentally observed transitions to the centric form.

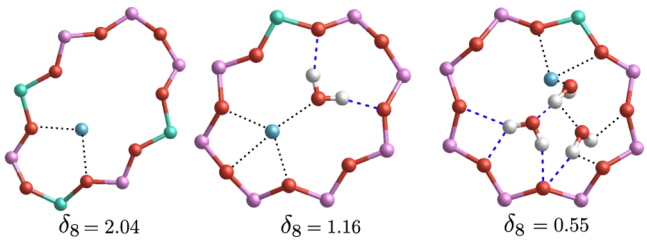

Figure 12. Snapshots of several 8MRs during simulations when occupied by one Na^+ cation (left), one Na^+ cation and one water molecule (middle), and one Na^+ cation and three water molecules (right). Note the gradual decrease of the instantaneous distortion parameter upon water presence. Blue dashed lines represent hydrogen bonds, and black-dotted lines represent other strong interactions.

CONCLUSIONS

A detailed investigation has been conducted to reach a better understanding of the distortion mechanisms that take place in molecular valve zeolite RHO. To the best of our knowledge, this is the first study that has addressed the behavior of zeolite molecular valves from a theoretical point of view. For this purpose, we have developed a new methodology based on cycles of MC calculations, EM, and MD simulations to study both monovalent and divalent cation-containing zeolite RHO and its evolution upon changes on the nature of EFCs, temperature, and adsorbed molecules. The explicit consideration of the polarizability of the oxygen atoms has been found to be necessary, and it has been taken into account by using the shell model.

The analysis of the ring distortions shows that there is a close relationship between the flexibility of the zeolite framework and the location of the EFCs, as well as the water molecules, thus providing an atomistic insight that goes beyond the experimental information obtained by diffraction techniques, as no symmetry restrictions are considered. This finding is likely to have an influence on the further understanding of diffusion and separation processes, which are controlled by the molecular valve effect arising from the windows distortions. Previous theoretical works have stressed the relation between the effective diameter of the windows and the flexibility of the framework, in pure silica zeolites, but how the framework is affected by the presence of EFCs had remained unexplored so far, being thus this work also pioneer in this respect. The analysis of the results obtained in our study enables us to draw the following conclusions concerning the structural features: (a) the phase transition from the centric to the acentric form of zeolite RHO is due to the force exerted by the EFCs, which has a similar effect to applying an external pressure, (b) the newly developed method is accurate enough to provide the cell parameters within 0.07−0.2% with respect to experimental values; (c) the cation sites are not only well located by our computational approach, but also their populations are in agreement with experiments; (d) a clear dependence on the polarizing power of the EFC has been found for the distortions of the 8MRs as well as the minimun aperture of these rings that control the nanovalve effect; (e) the distortions of 6MR and 8MR are connected, which explains the experimental observation that the largest distortion occurs for Li^+; (f) the 8MR distortions follow a different behavior with temperature depending on the nature of the EFC; (g) cations face large energy barriers to pass from one site to another when the zeolite is dehydrated, being particularly high in the case of divalent cations; (h) the amount of water present in the zeolite controls the population of cationic sites, the size of the cell parameters, and the symmetry of the zeolite; and (i) the 8MR windows distortion and pore aperture can be systematically controlled by the loading of water, allowing a fine control of the nanovalve effect.

The calculated high energy barriers for cation hopping provide a rationalization of the experimental finding that upon CO_2 adsorption in Cs-, NaCs-, and K-RHO, two crystal phases appear over a considerable range of gas pressures, which according to our results is a consequence of the trapping of sets of cations in a range of configurations that lead to long-lived metastable structures. We have shown that polar molecules, in

DOI: 10.1021/acs.chemmater.5b02103
Chem. Mater. 2015, 27, 5657−5667

this case water, screen the large electrostatic interaction providing low energy paths for the structural change.

■ ASSOCIATED CONTENT

Supporting Information

Initial and final structures for each metal at 300 K. Variation of the potential energy and cell size with the number of MD simulation steps, for ten MC/EM/MD cycles, for Na-RHO, Li-RHO, K-RHO, Sr-RHO, and Ca-RHO. MD NPT of a pure silica system computed by DFT. Avoiding the Buckingham catastrophe. The Supporting Information is available free of charge on the ACS Publications website at DOI: 10.1021/acs.chemmater.5b02103.

■ AUTHOR INFORMATION

Corresponding Authors

*E-mail: said@upo.es. Phone: +34 954 978312.
*E-mail: scalero@upo.es.

Notes

The authors declare no competing financial interest.

■ ACKNOWLEDGMENTS

This work is supported by the European Research Council through an ERC Starting Grant (Sofía Calero, ERC2011-StG-279520-RASPA), by the MINECO (Sofía Calero, CTQ2013-48396-P) by the Andalucía Region (Sofía Calero, FQM-1851), and by The Netherlands Council for Chemical Sciences (NWO/CW), through a VIDI grant (David Dubbeldam).

■ REFERENCES

(1) Meng, H.; Xue, M.; Xia, T.; Zhao, Y.-L.; Tamanoi, F.; Stoddart, J. F.; Zink, J. I.; Nel, A. E. Autonomous in Vitro Anticancer Drug Release from Mesoporous Silica Nanoparticles by pH-Sensitive Nanovalves. *J. Am. Chem. Soc.* **2010**, *132*, 12690−12697.

(2) Yang, Y.-W. Towards biocompatible nanovalves based on mesoporous silica nanoparticles. *MedChemComm* **2011**, *2*, 1033−1049.

(3) Yuan, Q.; Zhang, Y.; Chen, T.; Lu, D.; Zhao, Z.; Zhang, X.; Li, Z.; Yan, C.-H.; Tan, W. Photon-Manipulated Drug Release from a Mesoporous Nanocontainer Controlled by Azobenzene-Modified Nucleic Acid. *ACS Nano* **2012**, *6*, 6337−6344.

(4) Bernardos, A.; Mondragón, L.; Aznar, E.; Marcos, M. D.; Martínez-Máñez, R.; Sancenón, F.; Soto, J.; Barat, J. M.; Pérez-Payá, E.; Guillem, C.; Amorós, P. Enzyme-Responsive Intracellular Controlled Release Using Nanometric Silica Mesoporous Supports Capped with Saccharides. *ACS Nano* **2010**, *4*, 6353−6368.

(5) Kuznicki, S. M.; Bell, V. A.; Nair, S.; Hillhouse, H. W.; Jacubinas, R. M.; Braunbarth, C. M.; Toby, B. H.; Tsapatsis, M. A titanosilicate molecular sieve with adjustable pores for size-selective adsorption of molecules. *Nature* **2001**, *412*, 720−724.

(6) Corbin, D. R.; Abrams, L.; Jones, G. A.; Eddy, M. M.; Harrison, W. T. A.; Stucky, G. D.; Cox, D. E. Flexibility of the zeolite RHO framework: in situ x-ray and neutron powder structural characterization of divalent cation-exchanged zeolite RHO. *J. Am. Chem. Soc.* **1990**, *112*, 4821−4830.

(7) Parise, J. B.; Liu, X.; Corbin, D. R. Flexibility of the zeolite RHO framework; relocation of cadmium accompanying transformation of the unit cell at high temperatures. *J. Chem. Soc., Chem. Commun.* **1991**, 162−163.

(8) Reisner, B. A.; Lee, Y.; Hanson, J. C.; Jones, G. A.; Parise, J. B.; Corbin, D. R.; Toby, B. H.; Freitag, A.; Larese, J. Z.; Kahlenberg, V. Understanding negative thermal expansion and 'trap door' cation relocations in zeolite rho. *Chem. Commun.* **2000**, 2221−2222.

(9) Parise, J. B.; Cox, D. E. Structural changes occurring upon dehydration of zeolite Rho. A study using neutron powder diffraction and distance-least-squares structural modeling. *J. Phys. Chem.* **1984**, *88*, 1635−1640.

(10) Lee, Y.; Hriljac, J. A.; Vogt, T.; Parise, J. B.; Edmondson, M. J.; Anderson, P. A.; Corbin, D. R.; Nagai, T. Phase Transition of Zeolite RHO at High-Pressure. *J. Am. Chem. Soc.* **2001**, *123*, 8418−8419.

(11) Parise, J. B.; Abrams, L. E.; Gier, T.; Corbin, D. R.; Jorgensen, J. D.; Prince, E. Flexibility of the framework of zeolite Rho. Structural variation from 11 to 573 K. A study using neutron powder diffraction data. *J. Phys. Chem.* **1984**, *88*, 2303−2307.

(12) Palomino, M.; Corma, A.; Jorda, J. L.; Rey, F.; Valencia, S. Zeolite Rho: a highly selective adsorbent for CO_2/CH_4 separation induced by a structural phase modification. *Chem. Commun.* **2012**, *48*, 215−217.

(13) Lozinska, M.; Mangano, E.; Mowat, J.; Shepherd, A.; Howe, R.; Thompson, S.; Parker, J.; Brandani, S.; Wright, P. Understanding Carbon Dioxide Adsorption on Univalent Cation Forms of the Flexible Zeolite Rho at Conditions Relevant to Carbon Capture from Flue Gases. *J. Am. Chem. Soc.* **2012**, *134*, 17628−17642.

(14) Parise, J. B.; Prince, E. The structure of cesium-exchanged zeolite-Rho at 293K and 493K determined from high resolution neutron powder data. *Mater. Res. Bull.* **1983**, *18*, 841−852.

(15) Balestra, S. R. G.; Gutierrez-Sevillano, J. J.; Merkling, P. J.; Dubbeldam, D.; Calero, S. Simulation Study of Structural Changes in Zeolite RHO. *J. Phys. Chem. C* **2013**, *117*, 11592−11599.

(16) Baur, W.; Fischer, R.; Shannon, R. Relations and Correlations in Zeolite RHO and Computer Simulations of its Crystal Structure. *Innovation in Zeolite Materials Science Proceedings of an International Symposium* **1988**, *37*, 281−292.

(17) Bieniok, A.; Hammonds, K. D. Rigid unit modes and the phase transition and structural distortions of zeolite rho. *Microporous Mesoporous Mater.* **1998**, *25*, 193−200.

(18) Bieniok, A.; Baur, W. H. A large volume contraction accompanies the low- to high-temperature phase transition of zeolite Sr-rho. *J. Solid State Chem.* **1991**, *90*, 173−177.

(19) Mellot, C.; Lignieres, J. Monte Carlo Simulations of N_2 and O_2 Adsorption in Silicalite and CaLSX Zeolites. *Mol. Simul.* **1997**, *18*, 349−365.

(20) Vitale, G.; Mellot, C. F.; Bull, L. M.; Cheetham, A. K. Neutron Diffraction and Computational Study of Zeolite NaX: Influence of SIII′ Cations on Its Complex with Benzene. *J. Phys. Chem. B* **1997**, *101*, 4559−4564.

(21) Maurin, G.; Llewellyn, P.; Poyet, T.; Kuchta, B. Influence of Extra-Framework Cations on the Adsorption Properties of X-Faujasite systems: Microcalorimetry and Molecular Simulations. *J. Phys. Chem. B* **2005**, *109*, 125−129.

(22) Plant, D. F.; Maurin, G.; Jobic, H.; Llewellyn, P. L. Molecular Dynamics Simulation of the Cation Motion upon Adsorption of CO2 in Faujasite Zeolite Systems. *J. Phys. Chem. B* **2006**, *110*, 14372−14378.

(23) Ruiz-Salvador, A. R.; Lewis, D. W.; Rubayo-Soneira, J.; Rodríguez-Fuentes, G.; Sierra, L. R.; Catlow, C. R. A. Aluminum distribution in low Si/Al zeolites: dehydrated Na-clinoptilolite. *J. Phys. Chem. B* **1998**, *102*, 8417−8425.

(24) Ruiz-Salvador, A. R.; Gómez, A.; Lewis, D. W.; Rodríguez-Fuentes, G.; Montero, L. Silicon-aluminium distribution in dehydrated calcium heulandite. *Phys. Chem. Chem. Phys.* **1999**, *1*, 1679−1685.

(25) Fois, E.; Gamba, A.; Tabacchi, G.; Quartieri, S.; Vezzalini, G. On the collective properties of water molecules in one-dimensional zeolitic channels. *Phys. Chem. Chem. Phys.* **2001**, *3*, 4158−4163.

(26) Allan, N. L.; Barrera, G. D.; Purton, J. A.; Sims, C. E.; Taylor, M. B. Ionic solids at elevated temperatures and/or high pressures: lattice dynamics, molecular dynamics, Monte Carlo and ab initio studies. *Phys. Chem. Chem. Phys.* **2000**, *2*, 1099−1111.

(27) Ruiz-Salvador, A. R.; Garcia-Sanchez, M. F.; O'Reilly-Lukin, M.; Lewis, D. W.; Gomez, A. Approaching the structure of heavily defective ionic oxides through atomistic modeling. *Phys. Status Solidi C* **2005**, *2*, 3521−3524.

DOI: 10.1021/acs.chemmater.5b02103
Chem. Mater. 2015, 27, 5657−5667

(28) Van Beest, B.; Kramer, G. J.; Van Santen, R. Force fields for silicas and aluminophosphates based on ab initio calculations. *Phys. Rev. Lett.* **1990**, *64*, 1955.
(29) Kramer, G.; Farragher, N.; Van Beest, B.; Van Santen, R. Interatomic force fields for silicas, aluminophosphates, and zeolites: Derivation based on ab initio calculations. *Phys. Rev. B: Condens. Matter Mater. Phys.* **1991**, *43*, 5068.
(30) Ramsahye, N. A.; Bell, R. G. Cation Mobility and the Sorption of Chloroform in Zeolite NaY: A Molecular Dynamics Study. *J. Phys. Chem. B* **2005**, *109*, 4738−4747.
(31) Sanders, M. J.; Leslie, M.; Catlow, C. R. A. Interatomic potentials for SiO2. *J. Chem. Soc., Chem. Commun.* **1984**, 1271−1273.
(32) Jackson, R.; Bell, R.; Catlow, C. Computer simulation studies of zeolite structure and stability. In *Studies in Surface Science and Catalysis: Recent Advances in Zeolite Science Proceedings of the 1989 Meeting of the British Zeolite Association*; Klinowski, J., Barrie, P. J., Eds.; Elsevier: Amsterdam, The Netherlands, 1989; Vol.52; pp 203−208.
(33) Jackson, R. A.; Catlow, C. R. A. Computer Simulation Studies of Zeolite Structure. *Mol. Simul.* **1988**, *1*, 207−224.
(34) Kučera, J.; Nachtigall, P. Coordination of alkali metal ions in ZSM-5: A combined quantum mechanics/interatomic potential function study. *Phys. Chem. Chem. Phys.* **2003**, *5*, 3311−3317.
(35) Robson, H.; Shoemaker, D.; Ogilvie, R.; Manor, P. Synthesis and crystal structure of zeolite rho−A new zeolite related to Linde Type A. *Advances in Chemistry*; American Chemical Society: Washington, DC, 1973; Vol. *121*, pp 106−115.
(36) McCusker, L. B.; Baerlocher, C. The effect of dehydration upon the crystal structure of zeolite rho. *Proc. 6th Int. Zeolite Conf.*, Reno, NV, 1984; pp 812−822.
(37) Gomez-Hortiguela, L.; Pinar, A. B.; Cora, F.; Perez-Pariente, J. Dopant-siting selectivity in nanoporous catalysts: control of proton accessibility in zeolite catalysts through the rational use of templates. *Chem. Commun.* **2010**, *46*, 2073−2075.
(38) Dempsey, E.; Kuehl, G. H.; Olson, D. H. Variation of the lattice parameter with aluminum content in synthetic sodium faujasites. Evidence for ordering of the framework ions. *J. Phys. Chem.* **1969**, *73*, 387−390.
(39) Ruiz-Salvador, A. R.; Grau-Crespo, R.; Gray, A. E.; Lewis, D. W. Aluminium distribution in ZSM-5 revisited: The role of Al-Al interactions. *J. Solid State Chem.* **2013**, *198*, 330−336.
(40) Ruiz-Salvador, A. R.; Almora-Barrios, N.; Gómez, A.; Lewis, D. W. Interplay of water, extra-framework cations and framework atoms in the structure of low-silica zeolites: the case of the natural zeolite Goosecreekite as studied by computer simulation. *Phys. Chem. Chem. Phys.* **2007**, *9*, 521−532.
(41) Lozinska, M. M.; Mowat, J. P. S.; Wright, P. A.; Thompson, S. P.; Jorda, J. L.; Palomino, M.; Valencia, S.; Rey, F. Cation Gating and Relocation during the Highly Selective Trapdoor Adsorption of CO2 on Univalent Cation Forms of Zeolite Rho. *Chem. Mater.* **2014**, *26*, 2052−2061.
(42) White, C. L.; Ruiz-Salvador, A. R.; Lewis, D. W. Pressure-Induced Hydration Effects in the Zeolite Laumontite. *Angew. Chem.* **2004**, *116*, 475−478.
(43) Ruiz-Salvador, A. R.; Gómez, A.; Diaz, B.; Y, O.; Lewis, D. Si atoms in SAPO-31: A computational study. *Recent Advances in the Science and Technology of Zeolites and Related Materials Part B Proceedings of the 14th International Zeolite Conference*, 2004; Vol. *154* (Part B), pp 1439−1447.
(44) Jordá, J. L.; Rey, F.; Sastre, G.; Valencia, S.; Palomino, M.; Corma, A.; Segura, A.; Errandonea, D.; Lacomba, R.; Manjón, F. J.; Gomis, O.; Kleppe, A. K.; Jephcoat, A. P.; Amboage, M.; Rodríguez-Velamazán, J. A. Synthesis of a Novel Zeolite through a Pressure-Induced Reconstructive Phase Transition Process. *Angew. Chem., Int. Ed.* **2013**, *52*, 10458−10462.
(45) Domínguez-García, V.; Pigolotti, S.; Muñoz, M. A. Inherent directionality explains the lack of feedback loops in empirical networks. *Sci. Rep.* **2014**, *4*, 7497.
(46) Landau, L.; Lifshitz, E.; Sykes, J.; Kearsley, J. Course of Theoretical Physics. *Statistical Physics*; Elsevier Science: Amsterdam, The Netherlands, 1980.
(47) Frenkel, D.; Smit, B. *Understanding Molecular Simulation*, 2nd ed.; Academic Press: San Diego, CA, 2002.
(48) Dubbeldam, D.; Calero, S.; Ellis, D. E.; Snurr, R. Q. RASPA: molecular simulation software for adsorption and diffusion in flexible nanoporous materials. *Mol. Simul.* **2015**, *0*, 1−21.
(49) Gale, J. D.; Rohl, A. L. The General Utility Lattice Program (GULP). *Mol. Simul.* **2003**, *29*, 291−341.
(50) Parrinello, M.; Rahman, A. Polymorphic transitions in single crystals: A new molecular dynamics method. *J. Appl. Phys.* **1981**, *52*, 7182−7190.
(51) Ewald, P. Die berechnung optischer und elektrostatischer Gitterpotentiale. *Ann. Phys.* **1921**, *369*, 253.
(52) Adams, D. On the use of the Ewald summation in computer-simulation. *J. Chem. Phys.* **1983**, *78*, 2585.
(53) Loeweinstein, W. The distribution of aluminum in the tetrahedra of silicates and aluminates. *Am. Mineral.* **1954**, *39*, 92−96.
(54) Chandler, D. *Introduction to Modern Statistical Mechanics*; Oxford University Press: Oxford, U.K., 1987; Vol. *1*.
(55) Landau, L. D.; Lifshitz, E. M. *Course of Theoretical Physics*; Elsevier: Amsterdam, The Netherlands, 2013.
(56) Awati, R. V.; Ravikovitch, P. I.; Sholl, D. S. Efficient and Accurate Methods for Characterizing Effects of Framework Flexibility on Molecular Diffusion in Zeolites: CH_4 Diffusion in Eight Member Ring Zeolites. *J. Phys. Chem. C* **2013**, *117*, 13462−13473.
(57) Sastre, G. Computational study of diffusion of propane in small pore acidic zeotypes AFX and AEI. *Catal. Today* **2014**, *226*, 25−36.
(58) Tatsumi, T.; Liu, S.-B.; Matsuhashi, H.; Katada, N. Acid-Base Catalysis Advanced Sciences and Spreading Applications to Solutions of Environmental, Resources and Energy Issues: ABC-7, 7th International Symposium on Acid-Base Catalysis, Tokyo, May 12-15, 2013. *Catal. Today* **2014**, *226*, 1−216.
(59) Deem, M. W.; Newsam, J. M.; Creighton, J. A. Fluctuations in zeolite aperture dimensions simulated by crystal dynamics. *J. Am. Chem. Soc.* **1992**, *114*, 7198−7207.

DOI: 10.1021/acs.chemmater.5b02103
Chem. Mater. 2015, 27, 5657−5667